05

Dynamic properties of heavy concrete grade B45 under shock loading

© P.O. Petrov,[1,3] A.S. Savinykh,[2] G.V. Garkushin,[2] I.A. Zhukov,[1] A.A. Kozulin,[1] S.V. Razorenov[2]

[1]Tomsk State University,
Tomsk, Russia
[2]Federal Research Center for Problems of Chemical Physics and Medical Chemistry, Russian Academy of Sciences,
Chernogolovka, Moscow region, Russia
[3]Soyuzbeton,
Tomsk, Russia
e-mail: kozulyn@ftf.tsu.ru

Received June 19, 2025
Revised August 7, 2025
Accepted August 7, 2025

In this study, cylindrical samples of the B45 heavyweight concrete with a diameter of 105 mm and lengths of 25–500 mm were subjected to shock compression loads of 3.8 GPa, induced using explosive plane-wave generators. Upon loading, the shock wave profiles were continuously recorded with a „VISAR“ laser interferometer. As a result, dependences of the shock wave attenuation on the sample length and the dynamic hardening coefficient were determined. In addition, the dynamic (spall) strengths were assessed for the concrete samples under both compressive and tensile loads.

Keywords: heavyweight concrete, shock wave, VISAR interferometer, strength, compression, tension, dynamic hardening coefficient.

DOI: 10.61011/TP.2026.03.63161.149-25

Introduction

Owing to its unique physical and mechanical properties, wide availability, and relatively low cost of components, concrete is currently regarded as an irreplaceable material for construction of large-scale load-bearing and protective structures operating under both static and intense dynamic loads. Heavyweight concrete is a composite material where a conglomerate consisting of filler particles (crushed stone, chips, sand) is bonded by cement stone. To prevent cracking and increase the strength of concrete during its production, various types of reinforcement and fibers of different shapes, sizes, and compositions (metals, polymers, etc.) are often added to the mixture [1–6].

The problem of characterizing the dynamic strength properties of concrete is associated with the need for a calculated prediction of the response of engineering structures to an explosion, high-speed impact, and other intense pulse loads [7–9]. Studies into dynamic strength are focused largely on determining the corresponding strain rate dependence of strength [10]. Concrete is a brittle material with its tensile strength being many times lower than the compressive strength and pre-fracture plastic deformation being insignificant (or zero). The modified Kolsky method with a split-Hopkinson pressure bar [11] is the one that is used most frequently in world practice for assessing the strength of structural materials at strain rates up to $10^3\,s^{-1}$. The results of a series of experimental and theoretical studies into the strength properties of brittle materials (in particular, fine-grained concrete and advanced fiber-reinforced concrete types) were reported in [12]. Methods for testing concrete under Hopkinson bar loading have already been developed and implemented. They differ in the way loads are produced, in characteristic dimensions of the specimens being tested, and in how their structure is taken into account.

Shock wave measurement methods are used to examine the strength of brittle materials (ceramics, minerals, glass) under explosive or high-speed impact conditions at strain rates greater than $10^4\,s^{-1}$ [13]. Under such loading conditions, the method providing the most comprehensive data on the resistance of test specimens to rapid deformation and fracture is the one based on recording and subsequent analysis of evolution (shape change) of the compression wave in the process of its propagation through the material. The values of spall strength (15−41 MPa) of concrete specimens with a thickness of 12.7 mm and different gravel fractions were determined in the elastic compression region in experiments with a light-gas gun [14]. A noticeable influence of strain rate on the dynamic behavior of dry and water-filled concrete was demonstrated in [15]. Data on the attenuation of a shock wave propagating in ⌀52 mm specimens with a thickness of 8.84 mm were used to evaluate the fracture toughness of concrete within the range of shock compression pressures of 1.5–3.5 GPa [16] A series of experiments with ⌀65 mm concrete specimens 20 mm in thickness were conducted in [17,18] to determine the maximum shear stresses. It was found that the shear strength depends more on the matrix than on the fillers. The authors of [19] have demonstrated the lack of influence of the filler size on the shock adiabat under compressive stresses ranging from 3 to 23 GPa.

It should be noted that these earlier studies have a disadvantage in that they were limited in the permissible range of specimen sizes [14,16–18,20] and are thus normally applicable only to fine-grained concrete. Data for small-sized test specimens are ill-suited for scaling the obtained properties to real structural elements and do not satisfy the requirements for representative volumes of materials with large inclusions. Alternative testing methods remain relevant in studies of the dynamic properties of conventional large-fraction materials, such as heavyweight concrete with large aggregates [21,22].

The aim of the present study was to determine the strength properties of large-sized cylindrical specimens of heavyweight concrete B45 (C35/45) under compression and tension and explosive loading conditions.

1. Tested material

Cylindrical heavyweight concrete specimens were prepared in the laboratory of the concrete plant of Soyuzbeton LLC (Tomsk). The formula for the production of a concrete mixture was set according to GOST 27006-2019 and included 380 kg of the binder component (Portland cement CEM 0 42.5N manufactured by Topkinsky cement LLC), 130 kg of ECOFIL-480 slag, 700 kg of construction sand, 1055 kg of crushed dense rock with a size range of 5−10 mm, 190 kg of purified mixing water, and improving additives. The prepared concrete mixture was poured into molds in the form of ⌀105 mm plastic pipes 500 mm in length, which was followed by short-term compaction on a vibrating table. A batch of specimens in the form of cubes $100 \times 100 \times 100$ mm in size and ⌀105 mm pellets with a thickness of 200 mm was produced additionally to assess the static compressive and tensile strength, respectively. The specimens were kept in laboratory conditions for more than 28 days for development of strength. Figure 1 shows the cross cut of a cylindrical blank. It can be seen that crushed rock is distributed evenly over the surface. Thus, it was concluded that its distribution throughout the volume is also uniform. No large pores or air pockets are visible in Fig. 1.

Concrete density $\rho_0 = 2460\,\text{kg/m}^3$ was determined by the hydrostatic weighing method using an ME204T analytical scale (Mettler Toledo). To prevent their saturation with water, the specimens were covered with a thin layer of polyvinyl acetate glue prior to measurements. The values of longitudinal and shear sound velocity were measured using the ultrasonic method with a transducer frequency of 2.5 MHz and were $c_l = (4663 \pm 0.03)$ m/s and $c_s = (2532 \pm 0.03)$ m/s, respectively. Measurements were carried out for 25-mm-long specimens. Bulk sound velocity c_b was calculated as $c_b = \sqrt{c_l^2 - 4c_s^2/3} = (3633 \pm 0.05)$ m/s.

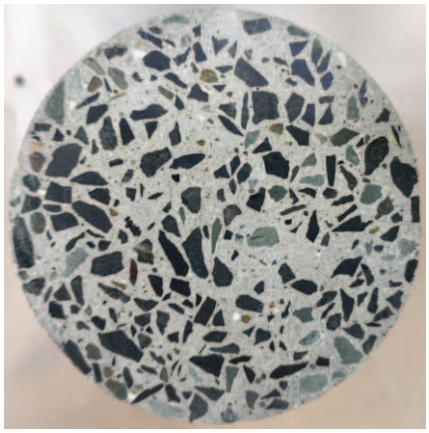

Figure 1. Ground surface of a ⌀105 mm concrete blank cut.

2. Experimental procedures

Experiments on the evaluation of static strength under compression and tension were carried out using a TP-1-1500 compression-testing machine in accordance with GOST 10180-2012 in the plant laboratory of Soyuzbeton LLC (Tomsk) at a loading rate of 0.6 MPa/s under axial compression of cubes and radial compression of ⌀105 mm pellets with a thickness of 200 mm in a Brazilian-type test [23]. The static compressive strength of prepared concrete turned out to be 59 MPa, which corresponds to heavyweight concrete grade B45; its tensile strength was 8 MPa.

Cylindrical specimens for shock-wave experiments with lengths of 200, 100, 70, 50, 35, and 25 mm were cut from 500-mm-long blanks using a diamond saw. To ensure plane-parallelism, the end surfaces of specimens were ground and polished with a diamond cup. The values of dynamic strength of the concrete specimens under study were determined in experiments on explosive loading performed according to the procedures detailed in [21,22,24] using test equipment provided by the Federal Research Center for Problems of Chemical Physics and Medical Chemistry of the Russian Academy of Sciences.

Figure 2 shows the diagram of the assembly for shock-wave experiments. A shock wave in a specimen was produced by detonation of plane-wave generator *1* 100 mm in diameter, which was placed in steel obturating ring *2* with a height of 27 mm and a wall thickness of 20 mm, to obtain the required pressure and duration of the shock compression pulse. The shock wave entered specimen *5* through screen *3* (detonation wave attenuator) made of polymethyl methacrylate with a thickness of 27 mm. This screen reduced the amplitude of the shock compression pulse formed by the explosive lens. The duration of the compression pulse at the attenuator output was more than 10 μs. The shock compression pressure was 3.8 GPa. Polarization sensor *4* was positioned between the screen (attenuator) and the specimen and used as a time marker

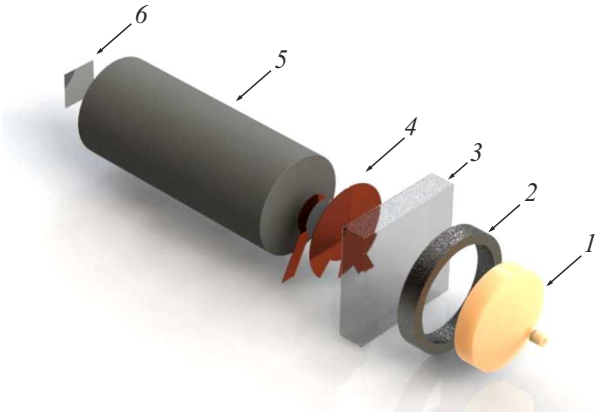

Figure 2. Exploded-view diagram of components of the assembly for a shock-wave experiment (see explanation in text).

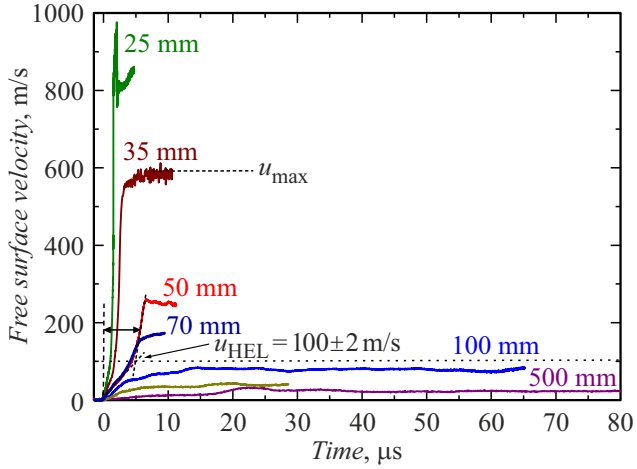

Figure 3. Experimental free surface velocity profiles of B45 concrete specimens with lengths from 25 to 500 mm. The numbers next to curves indicate the nominal specimen lengths.

of shock wave entry into the concrete specimen that is needed to measure the velocity of propagation of a shock compression pulse through the specimen. This sensor was a sandwich of copper foil (50 μm) — scotch tape (45 μm) — copper foil (50 μm) pressed tightly against each other. The scotch tape diameter was 45 mm. The operating principle of such sensors is referred to as impact polarization in literature [25]. The pressure jump between the plates (in the present case, copper with a polar dielectric — scotch tape) produced when the shock wave reaches the sensor is accompanied by the formation of EMF in the external circuit. The signal level reached in these experiments was on the order of 1 V.

Continuous recording of free surface velocity profiles $u_{fs}(t)$ of the specimens was carried out using a VISAR laser Doppler interferometric velocimeter [26]. Aluminum foil *6* with a thickness of 400 μm was glued with epoxy resin to the end surface of the specimen in order to reflect probing laser radiation.

3. Results of shock-wave experiments

Figure 3 shows the summarized profiles of the free surface velocity of B45 concrete specimens with lengths ranging from 25 to 500 mm. In concrete specimens 25–70 mm in length, the shock wave was found to be split into an elastic wave propagating with velocity U_{el} and a plastic one with velocity U_{pl}. Despite the significant duration of the initial shock compression pulse (more than 10 μs) entering the specimen, measurements revealed a significant reduction in amplitude of the plastic wave in the process of propagation of the compression wave in concrete. The drop in amplitude of the incident wave recorded in the wave profiles was observed not only in the plastic region of deformation in specimens with a length of 25–70 mm, but also during further propagation of the elastic wave along specimens with a length up to 500 mm. The width of the front of the plastic compression wave increased in the process of attenuation. No jump in parameters at the precursor front was noted; instead, a smooth velocity increase was observed in the elastic region, which implies that the material has no clearly defined dynamic elastic limit. Plastic deformation starts at the earliest stages of compression and is accompanied by strain hardening. This behavior is typical of concrete [12]. A certain contribution to hardening is made by the collapse of micropores in the specimen volume under impact compression of concrete.

Compressive stress σ_{HEL} behind the elastic precursor front corresponds to the dynamic elastic limit of concrete under uniaxial compression and is calculated using the following relation:

$$\sigma_{HEL} = \rho_0 c u_{HEL}/2, \tag{1}$$

where $c = 3957$ m/s is the propagation velocity of the elastic wave calculated for its middle part (since this wave diffuses as it propagates) and u_{HEL} is the elastic wave amplitude (Fig. 3). The calculated average σ_{HEL} value was (476 ± 30) MPa. The scatter of the obtained σ_{HEL} values is attributable to the complex composite structure of the specimens and microheterogeneities present in the specimen volume. The dynamic elastic limit measured in [14] for concrete specimens with a thickness of 12.74 mm was 550 MPa.

The maximum compressive stresses in the plastic deformation region for 25–70 mm specimens may be estimated using the following relation [27]:

$$\sigma_{\max} = \sigma_{HEL} + \rho_{el} U_{pl} \frac{(u_{\max} - u_{HEL})}{2}, \tag{2}$$

where ρ_{el} is the density in the elastic region calculated as

$$\rho_{el} = \frac{\rho_0 U_{pl}}{\left(U_{pl} - \frac{u_{HEL}}{2}\right)}. \tag{3}$$

Table 1. Results of experiments with B45 concrete

Designation	h_s, mm	u_{HEL}, m/s	σ_{HEL}, MPa	$u_{\max}$, m/s	$\sigma_{\max}$, GPa
25 mm	23.95	102.7	499	975.1	4.41
35 mm	35.9	92.2	447	576.7	2.58
50 mm	52.7	101.3	492	258.5	1.08
70 mm	69.8	96.1	467	168.3	0.79
100 mm	101.0	–	–	84.6	0.411
200 mm	201.0	–	–	46.2	0.224
500 mm	501.5	–	–	31.3	0.152

Note: h_s is the measured specimen length, u_{HEL} is the elastic wave amplitude, σ_{HEL} is the dynamic elastic limit, $u_{\max}$ is the maximum velocity in the $u_{fs}(t)$ profile, and $\sigma_{\max}$ is the maximum compressive stress.

Wave velocity U_{pl} is calculated in accordance with relation [13]

$$U_{pl} = \frac{h_s}{\left(\frac{h_s}{c_l} + \Delta t\right)}, \tag{4}$$

where Δt is the time difference between the moments when the middle part of the plastic part of the compression wave and the elastic part of the compression wave reach the free surface (Fig. 3). Plastic wave velocity U_{pl} does not depend on the specimen thickness (with the exception of the experiment with a 50 mm specimen, where a smaller U_{pl} value was obtained, which is likely attributable to the complex inhomogeneous structure of specimens). The maximum compressive stresses were estimated from the free surface velocity profile in the elastic deformation region for 100–500 mm specimens using the following relation:

$$\sigma_{\max} = \rho_0 c \frac{u_{\max}}{2}. \tag{5}$$

Figure 4 shows the dependence of the maximum compressive stress on thickness of B45 concrete specimens. The obtained dependence is divided into two sections: initial section of rapid attenuation I, which is the region of plastic deformation where the material undergoes fracture, and subsequent section of attenuation II of the elastic wave, which is accompanied by dissipative phenomena. The elastic–plastic transition stress is achieved in the process of compression wave attenuation at a specimen thickness slightly smaller than 100 mm. This is accompanied by an order-of-magnitude reduction in the maximum compressive stress. With further propagation of the elastic wave in the bar, $\sigma_{\max}$ decreases by a factor of 3. A significant attenuation of the shock wave from 2.5 to 0.5 GPa with an increase in thickness of concrete specimens to 18 mm was noted in experiments [16] where the duration of the incident compression pulse did not exceed 1 μs. Table 1 summarizes the experimental and calculated data obtained during shock-wave testing of B45 concrete specimens.

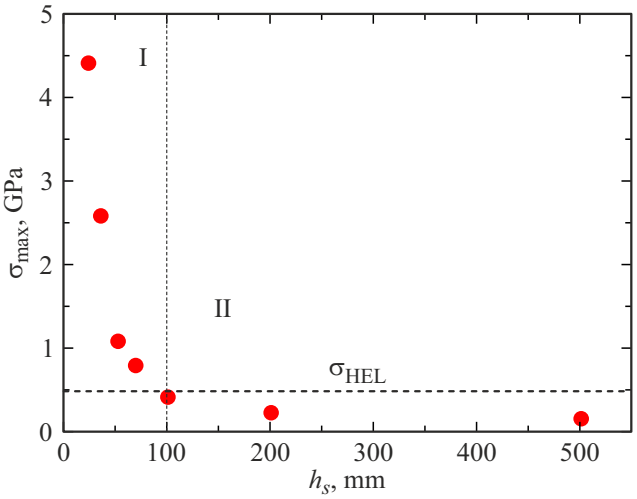

Figure 4. Dependences of the maximum compressive stress ($\sigma_{\max}$) on the specimen length (h_s).

4. Dynamic tensile and compressive strength

Figure 5 presents a photographic image of the remaining fragments of the 500-mm-long specimen after shock wave loading. Visual inspection of fragments of the preserved B45 concrete specimen after fracture revealed the presence of two types of fracture induced by tension (spall fracture) and compression along the entire length of 500 mm. The photograph makes it evident that the specimen subjected to tension split in several places perpendicular to the axis of the bar. Measured thickness L_{sp} of the spall fragment close to the end of the bar was 60–70 mm.

A fractured layer is seen at a distance of 70–100 mm from the end of the concrete bar. The end part has not been preserved. It was established that fracture under compression differs from fracture under tension in the shape of fragments facing the direction of propagation of the shock wave. The surviving blocks have no residual traces of plastic

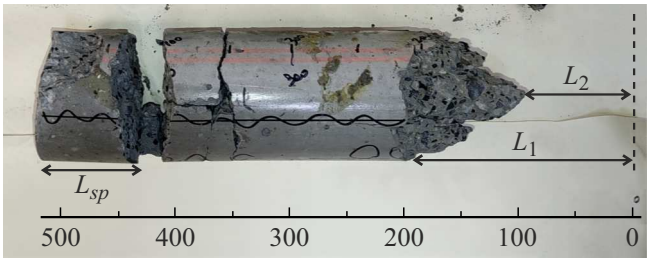

Figure 5. Fragments of a cylindrical B45 concrete specimen with a length of 500 mm after tests.

deformation. Visual inspection of the fragments revealed that the concrete specimen underwent fracture at distance L_1 (200 mm) with the formation of a conical shape at the beginning of the bar and without longitudinal cracks in the remaining parts. The compressive stress at a distance of 200 mm corresponds to the dynamic compressive strength of B45 concrete [21,22]. It can be seen from Fig. 5 that the specimen was destroyed completely at distance L_2 (100 mm).

Signs of spall fracture in the form of a part of the rarefaction wave reaching the specimen surface were noted in the process of recording the free surface velocity profiles for concrete specimens 100 and 200 mm in length (Fig. 6). A rarefaction wave may reach the surface only if the integrity of the specimen structure is maintained. The maximum free surface velocity for specimens 100 and 200 mm in length was 84.6 and 46.2 m/s, respectively, which is lower than the value of $u_{HEL} = (100 \pm 2)$ m/s (i.e., measurements were carried out in the elastic region). When dynamic elastic limit $\sigma_{HEL} = 467$ MPa and the maximum compressive stress $\sigma_{\max} = 411$ MPa are exceeded, concrete starts to fracture under compression, which is evidenced by the wave profiles obtained for specimens shorter than 100 mm (Fig. 3). No signs of spall fracture were found in the region of plastic deformation (Fig. 3). This behavior is typical of brittle materials such as sapphire [28]. The values of dynamic compressive strength of two types of concrete were obtained in a similar way in [21,22]. Since the slope of velocity gradient in the elastic compression wave in the experiment with the 70-mm-long specimen is similar to the slope in the experiment with the 100-mm-long specimen (Fig. 3), it may be assumed that the strain rates in the elastic wave are close. The corresponding strain rate may be determined using the relation

$$\frac{\dot{V}}{V_0} = \frac{\dot{u}_{fsc}}{2c} \sim 2200\,\mathrm{s}^{-1}, \tag{6}$$

where $\dot{u}_{fsc}$ is the velocity gradient in the compression wave.

The dynamic increase factor (DIF) of B45 concrete is the ratio of the compressive strength (411 MPa) under dynamic loading to the compressive strength under static loading (59 MPa). The DIF of B45 concrete under compression is on the order of 6–7, which is consistent with the data presented in [12].

Surface velocity decrement Δu_{fs} (Fig. 6), which is the difference between the maximum and minimum values of the free surface velocity in the unloading wave before spall fracture, is proportional to the magnitude of fracture stresses (spall strength of the material). In the linear acoustic approximation, the magnitude of tensile stresses acting at the moment of separation of the spall plate is calculated as

$$\sigma_{sp} = \rho_0 c \frac{\Delta u_{fs}}{2}, \tag{8}$$

where Δu_{fs} is the difference between the maximum and minimum values of the free surface velocity in the unloading wave. We determine the spall plate thickness from the free surface velocity profiles (Fig. 6) using the following relation [29]:

$$h_{sp} = \frac{\Delta t_{sp}}{\left(\frac{1}{c} + \frac{1}{U_{el}}\right)}, \tag{9}$$

where $\Delta t_{sp} = 30$–$40\,\mu$s is the duration of the loading pulse for the 500-mm-long specimen (the time between the end of spall fracture and reflection of the compression wave from the free surface). The thickness of the spall plate was calculated to be $h_{sp} = 64$ mm, which matches quite well the length of the preserved spall fragment (Fig. 5). Table 2 lists the calculated values of spall strength for specimens with a length of 100 mm and more.

The error in the obtained tensile strength values and the corresponding strain rates is estimated at 15 %–20 %. The scatter of the obtained results is attributable to the complex structure of specimens and the applied maximum stress $\sigma_{\max}$. It is fair to conclude that spall fracture occurs in the elastic region of deformation, which does not depend on the specimen length and the maximum compressive stress. Similar measurements of spall strength with variation of the maximum compressive stress were carried out in [14], and it was demonstrated that the spall strength of the

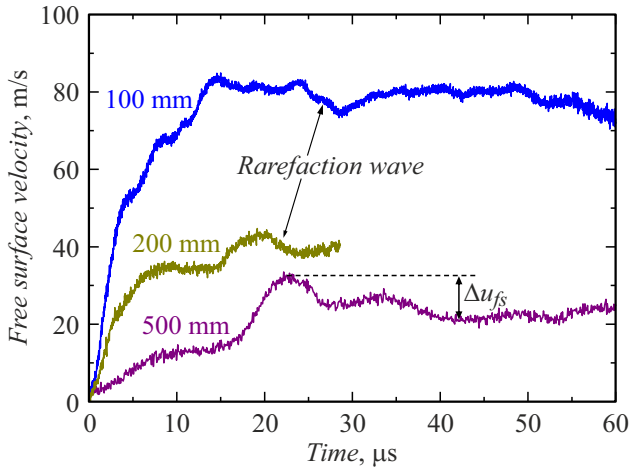

Figure 6. Enlarged free surface velocity profiles of B45 concrete specimens with a length of 100, 200, and 500 mm. Their nominal lengths are indicated. Arrows indicate the emergence of a part of the rarefaction wave.

Table 2. Dynamic tensile strength

Designation	h_s, mm	Δu_{fs}, m/s	σ_{sp}, MPa	$\dot{V}/V_0$, s^{-1}
100 mm	101.0	7.3	35.4	92
200 mm	201.0	4.8	23.3	126
500 mm	501.5	7.4	35.9	75

Note: Δu_{fs} is the difference between the maximum and minimum values of the free surface velocity in the unloading wave (Fig. 6), σ_{sp} is the spall strength, and V/V_0 is the strain rate in the rarefaction wave before spalling.

examined concrete with an approximate filler size of 10 mm does not depend on $\sigma_{\max}$ and reaches ~ 30 MPa within the range of maximum elastic compressive stresses of 83–553 MPa. Split-Hopkinson pressure bars were used in [30] to demonstrate that the spall strength of concrete with a filler size of 0.5–8 mm falls within the range of 7–12 MPa at strain rates of 60–130 s^{-1}. Measurements of the spall strength of MB50 concrete carried out in [15] revealed that $\sigma_{sp} = 14$–16 MPa. The spall strength of concrete made using granite chips is 8–10 MPa at strain rates of 30–50 s^{-1} [22]. The scatter of spall strength values at close strain rates is attributable to the difference in compositions and methods of preparation of the examined concrete specimens.

The DIF of the studied concrete under tension is 3–4, which is consistent with the data on the strength of concrete in [12].

Conclusion

The dynamic strength characteristics of B45 heavyweight concrete specimens in the form of ⌀105 mm bars with a length of 25-500 mm were measured experimentally with impact load pulses longer than 10 μs. Systematic studies of the evolution of shock compression pulses in bars were carried out. It was demonstrated that an elastic precursor with a smooth increase in stress at the wave front is formed under shock compression in specimens with a length of 25–70 mm. This elastic precursor is followed by a plastic shock wave. Strong attenuation of the plastic compression wave was observed in the process of pulse propagation through the specimen, while the elastic wave attenuation, which is accompanied by dissipative phenomena, was weak. Measurements of the compression pulse parameters at the boundary of the fracture zone and the elastic–plastic transition parameters provided an opportunity to determine the dynamic compressive strength of concrete. The estimated stresses at failure were in the range from $\sigma_{HEL} = 467$ to $\sigma_{\max} = 411$ MPa at a strain rate of ~ 2200 s^{-1}. The thickness of the remaining spall fragment was determined by analyzing the measured free surface velocity profile of the 500-mm-long concrete specimen. The tensile strength was ~ 30 MPa at a strain rate of ~ 100 s^{-1}. The dynamic increase factors under compression and tension were 6–7 and 3–4, respectively.

Funding

This study was supported by the Russian Science Foundation, grant № 25-29-00750, https://rscf.ru/project/25-29-00750.

Conflict of interest

The authors declare that they have no conflict of interest.

References

[1] C. Jiao, W. Sun, S. Huan, G. Jiang. Front. Archit. Civ. Eng. China, **3** (2), 131 (2009). DOI: 10.1007/s11709-009-0027-0
[2] M. Nili, A.H. Ghorbankhani, A. Alavi Nia, M. Zolfaghari. Construction and Building Mater., **107**, 264 (2016). DOI: 10.1016/j.conbuildmat.2015.12.161
[3] Z. Xu, H. Hao, H.N. Li. Appl. Mechan. Mater., **82**, 112 (2011). DOI: 10.4028/www.scientific.net/AMM.82.112
[4] Yu.M. Bazhenov. *Beton pri dinamicheskom nagruzhenii* (Stroiizdat, M., 1970) (in Russian)
[5] L. Coppola, E. Cadoni, D. Forni, A. Buoso. Appl. Mechan. Mater., **82**, 190 (2011). DOI: 10.4028/www.scientific.net/AMM.82.190
[6] A.M. Bragov, A.Y. Konstantinov, D.A. Lamzin, A.K. Lomunov, B.L. Karihaloo, Y.V. Petrov, I.V. Smirnov. J. Appl. Mechan. Tech. Phys., **53** (6), 926 (2012).
[7] A.M. Bragov, A.K. Lomunov, M.E. Gonov, A.Yu. Konstantinov, L.A. Igumnov, V.A. Eremeyev. Mater., **16** (6), 2259 (2023). DOI: 10.3390/ma16062259
[8] V.V. Karakulov, I.Y. Smolin, S.N. Kulkov. J. Phys.: Conf. Ser., **1045**, 012018 (2018). DOI: 10.1088/1742-6596/1045/1/012018
[9] A.V. Radchenko, P.A. Radchenko. *Udarno-volnovye protsessy i razrushenie v anizotropnykh materialakh i konstruktsiyakh* (Tomsk. Gos. Arkhit.-Stroit. Univ., Tomsk, 2015) (in Russian)
[10] N.V. Mikhailova, Yu.V. Petrov. Fiz. Mezomekh., **23** (3), 15 (2020) (in Russian).
[11] D.A. Lamzin, M.E. Gonov, A.M. Bragov, A.K. Lomunov. Vestn. Tomsk. Gos. Univ. Mat. Mekh., **81** (97), 97 (2023) (in Russian). DOI: 10.17223/19988621/81/9
[12] A.M. Bragov, L.A. Igumnov, A.K. Lomunov. *Vysokoskorostnaya deformatsiya melkozernistogo betona i fibrobetona* (Izd. Nizhegorod. Univ., Nizhnii Novgorod, 2015) (in Russian)
[13] G.I. Kanel, S.V. Razorenov, V.E. Fortov. *Shock-Wave Phenomena and the Properties of Condensed Matter* (Springer, NY., 2004), DOI: 10.1007/978-1-4757-4282-4
[14] M.E. Kipp, L.C. Chhabildas, W.D. Reinhart. AIP Conf. Proc., **429**, 557 (1998). DOI: 10.1063/1.55664
[15] P. Forquin, B. Erzar. Int. J. Fract., **163**, 193 (2010). DOI: 10.1007/s10704-009-9419-3
[16] j.-Y. Chen, C.-C. Liu, H.-W. Dong, D.-S. Shi, Z.-X. Zhang, D.J. Wang. Construction and Building Mater., **39**, 119 (2013). DOI: 10.1016/j.conbuildmat.2012.05.011

[17] K. Tsembelis, W.G. Proud. AIP Conf. Proc., **845**, 1496 (2006). DOI: 10.1063/1.2263608
[18] T. Andrews, D.J. Chapman, W.G. Proud. AIP Conf. Proc., **955**, 469 (2007). DOI: 10.1063/1.2833104
[19] C.A. Hall, L.C. Chhabildas, W.D. Reinhart. AIP Conf. Proc., **429**, 119 (1998). DOI: 10.1063/1.55638
[20] Y. Al-Salloum, T. Almusallam, S.M. Ibrahim, H. Abbas, S. Alsayed. Cement & Concrete Composites, **55**, 34 (2015). DOI: 10.1016/j.cemconcomp.2014.07.011
[21] A.S. Savinykh, G.V. Garkushin, G.I. Kanel, S.V. Razorenov. Int. J. Fract., **209**, 109 (2018). DOI: 10.1007/s10704-017-0244-9
[22] A.S. Savinykh, G.V. Garkushin, G.I. Kanel, S.V. Razorenov. Int. J. Fract., **215**, 129 (2019). DOI: 10.1007/s10704-018-00342-w
[23] ASTM C0496, Standard Test Method for Splitting Tensile Strength of Cylindrical Concrete Specimens, ASTM International, n. d., West Conshohocken, PA. DOI: 10.1520/C0496_C0496M-17
[24] G.I. Kanel', S.V. Razorenov, A.V. Utkin, V.E. Fortov. *Udarno-volnovye yavleniya v kondensirovannykh sredakh* (Yanus-K, M., 1996) (in Russian)
[25] V.N. Mineev, A.G. Ivanov. Sov. Phys. Usp., **19**, 400 (1976). DOI: 10.3367/UFNr.0119.197605c.0075
[26] L.M. Barker, R.E. Hollenbach. J. Appl. Phys., **43**, 4669 (1972). DOI: 10.1063/1.1660986
[27] E.B. Zaretsky, G.I. Kanel. J. Appl. Phys., **117**, 195901 (2015). DOI: 10.1063/1.4921356
[28] A.S. Savinykh, G.I. Kanel, S.V. Razorenov. Tech. Phys. Lett., **37** (7), 294 (2011). DOI: 10.1134/S1063785011040146
[29] T. Antoun, L. Seaman, D.R. Curran, G.I. Kanel, S.V. Razorenov, A.V. Utkin. *Spall Fracture* (Springer, NY., 2003), DOI: 10.1007/b97226
[30] P. Forquin, B. Lukić. J. Dynamic Behavior Mater., **4**, 34 (2018). DOI: 10.1007/s40870-017-0135-1

Translated by D.Safin